

Vijay PANCHORE¹

Meshless local Petrov-Galerkin method for rotating Rayleigh beam using Chebyshev and Legendre polynomials

Received 9 September 2021, Revised 17 January 2022, Accepted 25 January 2022, Published online 6 April 2022

Keywords: meshless local Petrov-Galerkin method, mechanical vibrations, orthogonal polynomials, Finite Element Method, rotating beams

The numerical solutions are obtained for rotating beams; the inclusion of centrifugal force term makes it difficult to get the analytical solutions. In this paper, we solve the free vibration problem of rotating Rayleigh beam using Chebyshev and Legendre polynomials where weak form of meshless local Petrov-Galerkin method is used. The equations which are derived for rotating beams result in stiffness matrices and the mass matrix. The orthogonal polynomials are used and results obtained with Chebyshev polynomials and Legendre polynomials are exactly the same. The results are compared with the literature and the conventional finite element method where only first seven terms of both the polynomials are considered. The first five natural frequencies and respective mode shapes are calculated. The results are accurate when compared to literature.

1. Introduction

The conventional finite element method is generally used for the partial differential equations for which analytical solutions are not possible. The solutions are first obtained in space and then in time; for free vibration problem of rotating beams the partial differential equations are first converted into ordinary differential equations where analytical solutions are not possible and then conventional finite element method is used. The inclusion of centrifugal force, in the governing

✉ Vijay Panchore, e-mail: vijaypanchore36@gmail.com

¹Department of Mechanical Engineering, Maulana Azad National Institute of Technology, Bhopal, India



© 2022. The Author(s). This is an open-access article distributed under the terms of the Creative Commons Attribution-NonCommercial-NoDerivatives License (CC BY-NC-ND 4.0, <https://creativecommons.org/licenses/by-nc-nd/4.0/>), which permits use, distribution, and reproduction in any medium, provided that the Article is properly cited, the use is non-commercial, and no modifications or adaptations are made.

differential equation of rotating beam, makes it difficult to obtain the analytical solution. In rotating beam literature, the solutions are available with conventional and improved finite element methods [1, 2]. The meshless method is an alternative to conventional finite element method where the weak form is written for a node and algebraic equations are obtained with assembled matrices [3, 4].

The meshless methods can then be defined in Galerkin and Petrov-Galerkin weak forms; for Galerkin method the procedure is similar to conventional finite element method but for Petrov-Galerkin method, two algebraic equations are written for each node and it is called the truly meshless method. The assembly of matrices is different for both the methods. The procedure in the truly meshless method results in two stiffness matrices including the boundary stiffness matrix. These solutions are useful in the case of a crack problem within the beams, and in the cases of high deformation where the elements can be distorted. The combinations of the trial and test function further improve the method.

The trial and test functions are chosen separately in the meshless method unlike conventional FEM. Here, the trial functions are assumed as the moving least squares function and the radial basis function. The test functions are chosen separately, one of the example is B-spline function. In radial basis function, the essential boundary condition is easily applied in the matrices as it satisfies the Kronecker delta property [5]. The number of nodes selected in one sub-domain can be limited, unlike conventional FEM, and depends on the function we choose. The assembly includes two rows for one node and results are accurate enough. The method can be explored with other functions as well, where there is a possibility of increasing the number of nodes within the sub-domain of the trial function [6, 7]. The Gaussian radial basis functions are generally used where higher-order derivatives are possible [8, 9].

In rotating beam literature, three beam theories are generally considered: the Euler-Bernoulli theory, the Timoshenko theory and the Rayleigh theory. The higher order Gaussian radial basis functions are useful while solving the Timoshenko beam problem where the problem of shear locking is explained. In Timoshenko beam, the rotary inertia and shear deformation are considered while in the case of Rayleigh beam only rotary inertia is considered in addition to the Euler-Bernoulli beam theory. In literature, these problems are explained. The numerical solutions of all these rotating beams provide the natural frequencies and mode shapes; based on the dimensions of the beam a theory can be selected.

The helicopter blades and turbines can be modeled with rotating beams; the solutions provide natural frequencies and the deflection of beams [10]. Generally, the numerical solutions of rotating beams are obtained with finite element method [11–14]. The traditional Galerkin method has also been used to solve the rotating beam problem [15]. The semi-analytical solutions are explored as well [16]. The differential equation has been solved using series solutions. The solutions are obtained with the new stiff-string polynomials as well [17]. The meshless methods, quadratic B-spline method is used to solve the rotating Euler-Bernoulli beam prob-

lem and the rotating beam problem [18, 19]; along with this, various structural problems have been solved [20].

The weak forms of meshless methods are the Galerkin method and other approaches where radial basis functions are explored along with moving least square basis functions [21–24]. In this paper, the rotating Rayleigh beam problem is solved using the Meshless local Petrov-Galerkin method where orthogonal polynomials, Chebyshev and Legendre, are used as a basis function. These polynomials are relatively much easier for computation when compared to radial basis functions and moving least squares basis function. The results are found very accurate, when compared to literature [25] where dynamic stiffness method is used, while considering only seven nodes within the one sub-domain of trial function. The results are obtained for different parameters available in literature. The results provide first five natural frequencies and mode shapes of a rotating Rayleigh beam.

2. Governing differential equation of a rotating beam

The Governing differential equation of a rotating Rayleigh beam is given by

$$\begin{aligned} \frac{\partial^2}{\partial x^2} \left[EI(x) \frac{\partial^2 w(x, t)}{\partial x^2} \right] + \rho A(x) \frac{\partial^2 w(x, t)}{\partial t^2} - \frac{\partial}{\partial x} \left[G(x) \frac{\partial w(x, t)}{\partial x} \right] \\ + \frac{\partial}{\partial x} \left\{ \rho I(x) \frac{\partial}{\partial x} \left[\Omega^2 w(x, t) - \frac{\partial^2 w(x, t)}{\partial t^2} \right] \right\} = 0, \quad (1) \end{aligned}$$

where, $EI(x)$ is the stiffness, ρ is the density, $A(x)$ is cross sectional area, $w(x)$ is the transverse displacement and $G(x)$ is the centrifugal force which is given by

$$G(x) = \int_x^R \rho A(x) \Omega^2 x dx. \quad (2)$$

Here, Ω is the angular velocity and R is the radius of the rotating beam.

For free vibration problem, we assume $w(x, t) = e^{i\omega t} \bar{w}(x)$ and get

$$\begin{aligned} \frac{d^2}{dx^2} \left[EI(x) \frac{d^2 \bar{w}(x)}{dx^2} \right] - \omega^2 \rho A(x) \bar{w}(x) - \frac{d}{dx} \left[G(x) \frac{d \bar{w}(x)}{dx} \right] \\ + \frac{d}{dx} \left\{ \rho I(x) \frac{d}{dx} \left[(\Omega^2 + \omega^2) \bar{w}(x) \right] \right\} = 0. \quad (3) \end{aligned}$$

The weak form is given by

$$\int_0^R v(x) \left\{ \frac{d^2}{dx^2} \left[EI(x) \frac{d^2 \bar{w}(x)}{dx^2} \right] - \rho A(x) \omega^2 \bar{w}(x) - \frac{d}{dx} \left[G(x) \frac{d \bar{w}(x)}{dx} \right] \right\} dx + \int_0^R v(x) \frac{d}{dx} \left\{ \rho I(x) \frac{d}{dx} \left[(\Omega^2 + \omega^2) \bar{w}(x) \right] \right\} = 0. \quad (4)$$

Integration by parts of Eq. (4) gives us

$$\left. v(x) \left\{ \frac{d}{dx} \left[EI(x) \frac{d^2 \bar{w}(x)}{dx^2} \right] - G(x) \frac{d \bar{w}(x)}{dx} + \rho I(x) \frac{d}{dx} \left[(\Omega^2 + \omega^2) \bar{w}(x) \right] \right\} \right|_0^R - \left. \frac{dv(x)}{dx} EI(x) \frac{d^2 \bar{w}(x)}{dx^2} \right|_0^R + \int_0^R EI(x) \frac{d^2 v(x)}{dx^2} \frac{d^2 \bar{w}(x)}{dx^2} dx + \int_0^R G(x) \frac{dv(x)}{dx} \frac{d \bar{w}(x)}{dx} dx - \Omega^2 \int_0^R \rho I(x) \frac{dv(x)}{dx} \frac{d \bar{w}(x)}{dx} dx - \omega^2 \int_0^R \rho A(x) v(x) \bar{w}(x) dx - \omega^2 \int_0^R \rho I(x) \frac{dv(x)}{dx} \frac{d \bar{w}(x)}{dx} dx = 0. \quad (5)$$

The natural boundary conditions are given by

$$\left\{ \frac{d}{dx} \left[EI(x) \frac{d^2 \bar{w}(x)}{dx^2} \right] - G(x) \frac{d \bar{w}(x)}{dx} + \rho I(x) \frac{d}{dx} \left[(\Omega^2 + \omega^2) \bar{w}(x) \right] \right\} \Big|_{(x=R)} = 0, \quad (6)$$

$$EI(x) \frac{d^2 \bar{w}(x)}{dx^2} \Big|_{(x=R)} = 0. \quad (7)$$

The Petrov-Galerkin equations for rotating Rayleigh beam are given by

$$\int_{\Omega_s} EI(x) \frac{d^2v}{dx^2} \frac{d^2\bar{w}}{dx^2} dx + \int_{\Omega_s} G(x) \frac{dv}{dx} \frac{d\bar{w}}{dx} dx - \omega^2 \int_{\Omega_s} \rho A(x) v \bar{w} dx - \Omega^2 \int_{\Omega^s} \rho I(x) \frac{dv(x)}{dx} \frac{d\bar{w}(x)}{dx} dx - \omega^2 \int_{\Omega^s} \rho A(x) v(x) \bar{w}(x) dx + \eta \left[\frac{d}{dx} \left(EI(x) \frac{d^2\bar{w}}{dx^2} \right) v - G(x) v \frac{d\bar{w}}{dx} + \rho I(x) \frac{d \left[(\Omega^2 + \omega^2) \bar{w}(x) v \right]}{dx} \right]_{\Omega_s \cap \Gamma_{\bar{w}}} - \eta \left[EI(x) \frac{dv}{dx} \frac{d^2\bar{w}}{dx^2} \right]_{\Omega_s \cap \Gamma_{\theta}} + \alpha_{\bar{w}} [(\bar{w} - \tilde{w}) v]_{\Omega_s \cap \Gamma_{\bar{w}}} + \alpha_{\theta} \left[\left(\frac{d\bar{w}}{dx} - \tilde{\theta} \right) \frac{dv}{dx} \right]_{\Omega_s \cap \Gamma_{\theta}} = 0. \quad (8)$$

Here, penalty parameters are given by $\alpha_{\bar{w}}$ and α_{θ} . η is a unit vector and it is positive on the right hand side of the sub-domain of the nodal test function. $\Omega_s \cap \Gamma_{\bar{w}}$ and $\Omega_s \cap \Gamma_{\theta}$ represent the intersection of the sub-domain of the nodal test function with the boundary, where deflection and slope are prescribed.

Here, Ω_s^i is the subdomain of test function, $\Gamma_s^{(i)}$ is the boundary of test function, $2S_v$ is the sub-domain length of test function, $2S_t$ is the sub-domain length of trial function. Fig. 1 shows the Petrov-Galerkin arrangement for rotating Rayleigh beam.

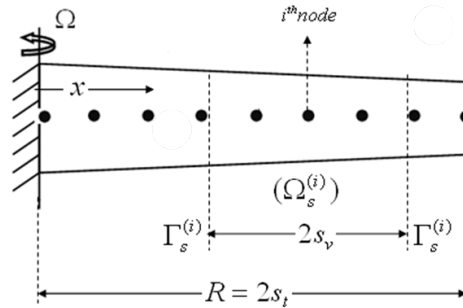


Fig. 1. Nodal distribution for MLPG method

3. Interpolation using Chebyshev and Legendre polynomials

The transverse displacement is given by

$$\bar{w}(x) = T_0(x)a_1 + T_1(x)a_2 + T_2(x)a_3 + \dots T_{2N-1}(x)a_{2N}. \quad (9)$$

The slope is given by

$$\theta(x) = \frac{dT_0(x)}{dx} a_1 + \frac{dT_1(x)}{dx} a_2 + \frac{dT_2(x)}{dx} a_3 + \dots \frac{dT_{2N-1}(x)}{dx} a_{2N}. \quad (10)$$

Eq. (9) and Eq. (10) can be written in matrix form as

$$\begin{bmatrix} \bar{w} \\ \theta \end{bmatrix} = \begin{bmatrix} T_0(x) & T_1(x) & \dots & T_{2N-1}(x) \\ \frac{dT_0(x)}{dx} & \frac{dT_1(x)}{dx} & \dots & \frac{dT_{2N-1}(x)}{dx} \end{bmatrix} \begin{bmatrix} a_1 \\ a_2 \\ \vdots \\ a_{2N} \end{bmatrix}. \quad (11)$$

Here, the Chebyshev polynomials are given by

$$T_0 = 1; \quad T_1 = x; \quad T_2 = 2x^2 - 1; \quad T_3 = 4x^3 - 3x; \quad T_4 = 8x^4 - 8x^2 + 1. \quad (12)$$

The recurrence relation is given by

$$T_{n+1}(x) = 2xT_n(x) - T_{n-1}(x). \quad (13)$$

The Legendre polynomials are given by

$$\begin{aligned} P_0 = 1; \quad P_1 = x; \quad P_2 = \frac{1}{2}(3x^2 - 1); \\ P_3 = \frac{1}{2}(5x^3 - 3x); \quad P_4 = \frac{1}{8}(35x^4 - 30x^2 + 3). \end{aligned} \quad (14)$$

The recurrence relation is given by

$$(n+1)P_{n+1}(x) = (2n+1)xP_n(x) - nP_{n-1}(x). \quad (15)$$

Substituting all the nodal values, we get

$$\begin{bmatrix} \bar{w}_1 \\ \theta_1 \\ \bar{w}_2 \\ \theta_2 \\ \vdots \\ \bar{w}_n \\ \theta_n \end{bmatrix} = \begin{bmatrix} T_0(x_1) & T_1(x_1) & \dots & T_{2N-1}(x_1) \\ \frac{dT_0(x_1)}{dx} & \frac{dT_1(x_1)}{dx} & \dots & \frac{dT_{2N-1}(x_1)}{dx} \\ T_0(x_2) & T_1(x_2) & \dots & T_{2N-1}(x_2) \\ \frac{dT_0(x_2)}{dx} & \frac{dT_1(x_2)}{dx} & \dots & \frac{dT_{2N-1}(x_2)}{dx} \\ \vdots & \vdots & \vdots & \vdots \\ T_0(x_N) & T_1(x_N) & \dots & T_{2N-1}(x_N) \\ \frac{dT_0(x_N)}{dx} & \frac{dT_1(x_N)}{dx} & \dots & \frac{dT_{2N-1}(x_N)}{dx} \end{bmatrix} \begin{bmatrix} a_1 \\ a_2 \\ \vdots \\ a_{2N-1} \\ a_{2N} \end{bmatrix}. \quad (16)$$

The left hand side vector represents transverse displacement and slope at respective nodes. The right hand side vector represents unknown constants which are used to formulate shape functions. The matrix consists of substitution of nodal values in Chebyshev and Legendre polynomials. Then we write

$$[d] = [R][a]. \quad (17)$$

Here, $[d]$ is a vector which consists of transverse displacement and slope. Where, \bar{w}_n is the displacement at n -th node and θ_n is the slope at n -th node. Or

$$[a] = [R]^{-1} [d]. \quad (18)$$

From Eq. (9) and Eq. (18) we get

$$\bar{w}(x) = [N] [d], \quad (19)$$

where, $[N]$ is the shape function and $\bar{w}(x)$ is the transverse displacement.

$$[N(x)]_{(1,2N)} = [\phi_1^{(w)}(x) \phi_1^{(\theta)}(x) \phi_2^{(w)}(x) \phi_2^{(\theta)}(x) \dots \phi_N^{(w)}(x) \phi_N^{(\theta)}(x)], \quad (20)$$

where, $\phi_i^{(w)}(x)$ and $\phi_i^{(\theta)}(x)$ are the shape functions for node i .

Then trial function can be written as

$$\bar{w}(x) = \sum_{j=1}^N (\phi_j^{(w)}(x) \bar{w}_j + \phi_j^{(\theta)}(x) \theta_j). \quad (21)$$

Only one sub-domain can be considered for the entire length of the rotating beam.

4. Selection of test function

The test function for node i is given by

$$\zeta_i^{(\bar{w})}(x) = \begin{cases} \left[1 - \left(\frac{|x - x_i|}{s_v} \right)^2 \right]^4 & 0 \leq |x - x_i| \leq s_v, \\ 0 & |x - x_i| > s_v, \end{cases} \quad (22)$$

$$\zeta_i^{(\theta)}(x) = \frac{d\zeta_i^{(\bar{w})}(x)}{dx}. \quad (23)$$

The complete test function is given by

$$v(x) = \delta \bar{w}_i \zeta_i^{(\bar{w})}(x) + \delta \theta_i \zeta_i^{(\theta)}(x). \quad (24)$$

Here, $\delta \bar{w}_i$ and $\delta \theta_i$ are chosen arbitrarily and will be eliminated in the formulation as we derive the stiffness matrix and mass matrix. Also, the test function is defined for the each node and then matrices can be assembled.

Fig. 2 and Fig. 3 show variation of test function and overlapping of sub-domain respectively.

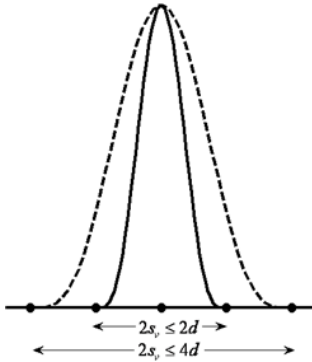


Fig. 2. Variation of test function

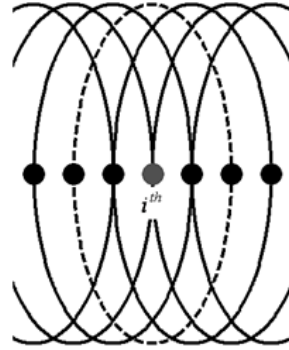


Fig. 3. Overlapping of sub-domain

5. Formulation of meshless Petrov-Galerkin method for a rotating Rayleigh beam

The formulation in meshless Petrov-Galerkin method includes two stiffness matrices: one is on the node and the second on boundary. The equations are written very clearly while the next steps are explained. The test and trial functions along with governing differential equation of a rotating Rayleigh beam result in the formulation.

$$\begin{aligned}
 & \sum_{j=1}^N \int_{\Omega_S^{(i)}} EI(x) \left(\delta \bar{w}_i \frac{d^2 \zeta_i^{(\bar{w})}}{dx^2} + \delta \theta_i \frac{d^2 \zeta_i^{(\theta)}}{dx^2} \right) \left(\frac{d^2 \phi_j^{(\bar{w})}}{dx^2} \bar{w}_j + \frac{d^2 \phi_j^{(\theta)}}{dx^2} \theta_j \right) dx \\
 & + \sum_{j=1}^N \int_{\Omega_S^{(i)}} G(x) \left(\delta \bar{w}_i \frac{d \zeta_i^{(\bar{w})}}{dx} + \delta \theta_i \frac{d \zeta_i^{(\theta)}}{dx} \right) \left(\frac{d \phi_j^{(\theta)}}{dx} \bar{w}_j + \frac{d \phi_j^{(\theta)}}{dx} \theta_j \right) dx \\
 & - \sum_{j=1}^N \omega^2 \int_{\Omega_S^{(i)}} \rho A(x) \left(\delta \bar{w}_i \zeta_i^{(\bar{w})} + \delta \theta_i \zeta_i^{(\theta)} \right) \left(\phi_j^{(\bar{w})} \bar{w}_j + \phi_j^{(\theta)} \theta_j \right) dx \\
 & - \sum_{j=1}^n \Omega^2 \int_{\Omega_S^{(i)}} \rho I(x) \left(\delta \bar{w}_i \frac{d \zeta_i^{(\bar{w})}}{dx} + \delta \theta_i \frac{d \zeta_i^{(\theta)}}{dx} \right) \left(\frac{d \phi_j^{(\theta)}}{dx} \bar{w}_j + \frac{d \phi_j^{(\theta)}}{dx} \theta_j \right) dx \\
 & - \sum_{j=1}^n \omega^2 \int_{\Omega_S^{(i)}} \rho I(x) \left(\delta \bar{w}_i \frac{d \zeta_i^{(\bar{w})}}{dx} + \delta \theta_i \frac{d \zeta_i^{(\theta)}}{dx} \right) \left(\frac{d \phi_j^{(\theta)}}{dx} \bar{w}_j + \frac{d \phi_j^{(\theta)}}{dx} \theta_j \right) dx
 \end{aligned}$$

$$\begin{aligned}
 & + \sum_{j=1}^N \eta \left[\begin{aligned}
 & EI(x_j) \left(\delta \bar{w}_i \zeta_i^{(\bar{w})} + \delta \theta_i \zeta_i^{(\theta)} \right) \left(\frac{d^3 \phi_j^{(\bar{w})}}{dx^3} \bar{w}_j + \frac{d^3 \phi_j^{(\theta)}}{dx^3} \theta_j \right) \\
 & + \frac{dEI(x_j)}{dx} \left(\delta \bar{w}_i \zeta_i^{(\bar{w})} + \delta \theta_i \zeta_i^{(\theta)} \right) \left(\frac{d^2 \phi_j^{(\bar{w})}}{dx^2} \bar{w}_j + \frac{d^2 \phi_j^{(\theta)}}{dx^2} \theta_j \right) \\
 & - G(x_j) \left(\delta \bar{w}_i \zeta_i^{(\bar{w})} + \delta \theta_i \zeta_i^{(\theta)} \right) \left(\frac{d\phi_j^{(\bar{w})}}{dx} \bar{w}_j + \frac{d\phi_j^{(\theta)}}{dx} \theta_j \right) \\
 & + \rho I(x) (\Omega^2 + \omega^2) \left(\delta \bar{w}_i \zeta_i^{(\bar{w})} + \delta \theta_i \zeta_i^{(\theta)} \right) \left(\frac{d\phi_j^{(\bar{w})}}{dx} \bar{w}_j + \frac{d\phi_j^{(\theta)}}{dx} \theta_j \right)
 \end{aligned} \right]_{\Omega_s^{(i)} \cap \Gamma_{\bar{w}}} \\
 & - \sum_{j=1}^N \eta \left[EI(x_j) \left(\delta \bar{w}_i \frac{d\zeta_i^{(\bar{w})}}{dx} + \delta \theta_i \frac{d\zeta_i^{(\theta)}}{dx} \right) \left(\frac{d^2 \phi_j^{(\bar{w})}}{dx^2} \bar{w}_j + \frac{d^2 \phi_j^{(\theta)}}{dx^2} \theta_j \right) \right]_{\Omega_s^{(i)} \cap \Gamma_{\theta}} \\
 & + \sum_{j=1}^N \alpha_{\bar{w}} \left[\left(\delta \bar{w}_i \zeta_i^{(\bar{w})} + \delta \theta_i \zeta_i^{(\theta)} \right) \left(\phi_j^{(\bar{w})} \bar{w}_j + \phi_j^{(\theta)} \theta_j - \bar{w} \right) \right]_{\Omega_s^{(i)} \cap \Gamma_{\bar{w}}} \\
 & + \sum_{j=1}^N \alpha_{\theta} \left[\left(\delta \bar{w}_i \frac{d\zeta_i^{(\bar{w})}}{dx} + \delta \theta_i \frac{d\zeta_i^{(\theta)}}{dx} \right) \left(\frac{d\phi_j^{(\bar{w})}}{dx} \bar{w}_j + \frac{d\phi_j^{(\theta)}}{dx} \theta_j - \tilde{\theta} \right) \right]_{\Omega_s^{(i)} \cap \Gamma_{\theta}} = 0. \quad (25)
 \end{aligned}$$

The complete weak form is obtained in Eq. (25). From the above expression we write stiffness matrix as

$$\begin{aligned}
 [K_{ij}]^{(\text{node})} & = \begin{bmatrix} \int_{\Omega_s^{(i)}} EI(x) \frac{d^2 \zeta_i^{(\bar{w})}}{dx^2} \frac{d^2 \phi_j^{(\bar{w})}}{dx^2} dx & \int_{\Omega_s^{(i)}} EI(x) \frac{d^2 \zeta_i^{(\bar{w})}}{dx^2} \frac{d^2 \phi_j^{(\theta)}}{dx^2} dx \\ \int_{\Omega_s^{(i)}} EI(x) \frac{d^2 \zeta_i^{(\theta)}}{dx^2} \frac{d^2 \phi_j^{(\bar{w})}}{dx^2} dx & \int_{\Omega_s^{(i)}} EI(x) \frac{d^2 \zeta_i^{(\theta)}}{dx^2} \frac{d^2 \phi_j^{(\theta)}}{dx^2} dx \end{bmatrix} \\
 & + \begin{bmatrix} \int_{\Omega_s^{(i)}} G(x) \frac{d\zeta_i^{(\bar{w})}}{dx} \frac{d\phi_j^{(\bar{w})}}{dx} dx & \int_{\Omega_s^{(i)}} G(x) \frac{d\zeta_i^{(\bar{w})}}{dx} \frac{d\phi_j^{(\theta)}}{dx} dx \\ \int_{\Omega_s^{(i)}} G(x) \frac{d\zeta_i^{(\theta)}}{dx} \frac{d\phi_j^{(\bar{w})}}{dx} dx & \int_{\Omega_s^{(i)}} G(x) \frac{d\zeta_i^{(\theta)}}{dx} \frac{d\phi_j^{(\theta)}}{dx} dx \end{bmatrix} \\
 & - \Omega^2 \begin{bmatrix} \int_{\Omega_s^{(i)}} \rho I(x) \frac{d\zeta_i^{(\bar{w})}}{dx} \frac{d\phi_j^{(\bar{w})}}{dx} dx & \int_{\Omega_s^{(i)}} \rho I(x) \frac{d\zeta_i^{(\bar{w})}}{dx} \frac{d\phi_j^{(\theta)}}{dx} dx \\ \int_{\Omega_s^{(i)}} \rho I(x) \frac{d\zeta_i^{(\theta)}}{dx} \frac{d\phi_j^{(\bar{w})}}{dx} dx & \int_{\Omega_s^{(i)}} \rho I(x) \frac{d\zeta_i^{(\theta)}}{dx} \frac{d\phi_j^{(\theta)}}{dx} dx \end{bmatrix}. \quad (26)
 \end{aligned}$$

Stiffness matrix at boundary is given by

$$\begin{aligned}
 [K_{ij}]^{(\text{bound})} &= \alpha_{\bar{w}} \begin{bmatrix} \zeta_i^{(\bar{w})} \phi_j^{(\bar{w})} & \zeta_i^{(\bar{w})} \phi_j^{(\theta)} \\ \zeta_i^{(\theta)} \phi_j^{(\bar{w})} & \zeta_i^{(\theta)} \phi_j^{(\theta)} \end{bmatrix}_{\Omega_s^{(i)} \cap \Gamma_{\bar{e}}} \\
 &+ \alpha_{\theta} \begin{bmatrix} \frac{d\zeta_i^{(\bar{w})}}{dx} \frac{d\phi_j^{(\bar{w})}}{dx} & \frac{d\zeta_i^{(\bar{w})}}{dx} \frac{d\phi_j^{(\theta)}}{dx} \\ \frac{d\zeta_i^{(\theta)}}{dx} \frac{d\phi_j^{(\bar{w})}}{dx} & \frac{d\zeta_i^{(\theta)}}{dx} \frac{d\phi_j^{(\theta)}}{dx} \end{bmatrix}_{\Omega_s^{(i)} \cap \Gamma_{\theta}} \\
 &+ \eta \begin{bmatrix} a_{11} & a_{12} \\ a_{21} & a_{22} \end{bmatrix}_{\Omega_s^{(i)} \cap \Gamma_{\bar{w}}} \\
 &- \eta \begin{bmatrix} EI(x_j) \frac{d\zeta_i^{(\bar{w})}}{dx} \frac{d^2\phi_j^{(\bar{w})}}{dx^2} & EI(x_j) \frac{d\zeta_i^{(\bar{w})}}{dx} \frac{d^2\phi_j^{(\theta)}}{dx^2} \\ EI(x_j) \frac{d\zeta_i^{(\theta)}}{dx} \frac{d^2\phi_j^{(\bar{w})}}{dx^2} & EI(x_j) \frac{d\zeta_i^{(\theta)}}{dx} \frac{d^2\phi_j^{(\theta)}}{dx^2} \end{bmatrix}_{\Omega_s^{(i)} \cap \Gamma_{\theta}}, \quad (27)
 \end{aligned}$$

where,

$$\begin{aligned}
 a_{11} &= EI(x_j) \zeta_i^{(\bar{w})} \frac{d^3\phi_j^{(\bar{w})}}{dx^3} + \frac{dEI(x_j)}{dx} \zeta_i^{(\bar{w})} \frac{d^2\phi_j^{(\bar{w})}}{dx^2} - G(x_j) \zeta_i^{(\bar{w})} \frac{d\phi_j^{(\bar{w})}}{dx} \\
 &+ \rho I(x) (\Omega^2 + \omega^2) \zeta_i^{(\bar{w})} \frac{d\phi_j^{(\bar{w})}}{dx}, \\
 a_{12} &= EI(x_j) \zeta_i^{(\bar{w})} \frac{d^3\phi_j^{(\theta)}}{dx^3} + \frac{dEI(x_j)}{dx} \zeta_i^{(\bar{w})} \frac{d^2\phi_j^{(\theta)}}{dx^2} - G(x_j) \zeta_i^{(\bar{w})} \frac{d\phi_j^{(\theta)}}{dx} \\
 &+ \rho I(x) (\Omega^2 + \omega^2) \zeta_i^{(\bar{w})} \frac{d\phi_j^{(\theta)}}{dx}, \\
 a_{21} &= EI(x_j) \zeta_i^{(\theta)} \frac{d^3\phi_j^{(\bar{w})}}{dx^3} + \frac{dEI(x_j)}{dx} \zeta_i^{(\theta)} \frac{d^2\phi_j^{(\bar{w})}}{dx^2} - G(x_j) \zeta_i^{(\theta)} \frac{d\phi_j^{(\bar{w})}}{dx} \\
 &+ \rho I(x) (\Omega^2 + \omega^2) \zeta_i^{(\theta)} \frac{d\phi_j^{(\bar{w})}}{dx}, \\
 a_{22} &= EI(x_j) \zeta_i^{(\theta)} \frac{d^3\phi_j^{(\theta)}}{dx^3} + \frac{dEI(x_j)}{dx} \zeta_i^{(\theta)} \frac{d^2\phi_j^{(\theta)}}{dx^2} - G(x_j) \zeta_i^{(\theta)} \frac{d\phi_j^{(\theta)}}{dx} \\
 &+ \rho I(x) (\Omega^2 + \omega^2) \zeta_i^{(\theta)} \frac{d\phi_j^{(\theta)}}{dx},
 \end{aligned}$$

The mass matrix is given by

$$\begin{aligned}
 [M_{ij}]^{(\text{node})} &= \begin{bmatrix} \int_{\Omega_s^{(i)}} \rho A(x) \zeta_i^{(\bar{w})} \phi_j^{(\bar{w})} dx & \int_{\Omega_s^{(i)}} \rho A(x) \zeta_i^{(\bar{w})} \phi_j^{(\theta)} dx \\ \int_{\Omega_s^{(i)}} \rho A(x) \zeta_i^{(\theta)} \phi_j^{(\bar{w})} dx & \int_{\Omega_s^{(i)}} \rho A(x) \zeta_i^{(\theta)} \phi_j^{(\theta)} dx \end{bmatrix} \\
 &+ \begin{bmatrix} \int_{\Omega_s^{(i)}} \rho I(x) \frac{d}{dx} (\zeta_i^{(\bar{w})} \phi_j^{(\bar{w})}) dx & \int_{\Omega_s^{(i)}} \rho I(x) \frac{d}{dx} (\zeta_i^{(\bar{w})} \phi_j^{(\theta)}) dx \\ \int_{\Omega_s^{(i)}} \rho I(x) \frac{d}{dx} (\zeta_i^{(\theta)} \phi_j^{(\bar{w})}) dx & \int_{\Omega_s^{(i)}} \rho I(x) \frac{d}{dx} (\zeta_i^{(\theta)} \phi_j^{(\theta)}) dx \end{bmatrix}. \quad (28)
 \end{aligned}$$

6. Non dimensional form of the equations

The results available in the literature are in non-dimensional form. The formulation is given by

$$I(x) = I_0 g(x), \quad (29)$$

$$A(x) = A_0 f(x), \quad (30)$$

where,

$$g(x) = \left(1 - c \frac{x}{R}\right)^{\bar{n}+2}, \quad (31)$$

$$f(x) = \left(1 - c \frac{x}{R}\right)^{\bar{n}}, \quad (32)$$

and c is a constant. Here, A_0 and I_0 are the uniform cross sectional area and second moment of area terms, respectively.

The non-dimensional form of the equation (1) is given by

$$\begin{aligned}
 \frac{d^2}{d\zeta^2} \left[g(\zeta) \frac{d^2 \bar{w}(\zeta)}{d\zeta^2} \right] - \lambda^2 f(\zeta) \bar{w}(\zeta) - s^2 \frac{d}{d\zeta} \left[h(\zeta) \frac{d \bar{w}(\zeta)}{d\zeta} \right] \\
 + \frac{s^2}{r^2} \frac{d}{d\zeta} \left[g(\zeta) \frac{d \bar{w}(\zeta)}{d\zeta} \right] + \frac{\lambda^2}{r^2} \frac{d}{d\zeta} \left[g(\zeta) \frac{d \bar{w}(\zeta)}{d\zeta} \right] = 0, \quad (33)
 \end{aligned}$$

where, $\zeta = \frac{x}{R}$, $r^2 = \frac{A_0 R^2}{I_0}$, $s^2 = \Omega^2 \frac{\rho A_0 R^4}{EI_0}$, $\lambda^2 = \omega^2 \frac{\rho A_0 R^4}{EI_0}$, and $h(\zeta) = \int_{\zeta}^1 \zeta f(\zeta) d\zeta$.

Here, s is the non-dimensional rotating speed, λ is the non-dimensional natural frequency, and r is the slenderness ratio which differentiates results of the Rayleigh

beam and the Euler-Bernoulli beam. For a thick beam, the results of both the theories tend to differ, but as the beam gets slender the difference is insignificant.

In non-dimensional form, the boundary conditions are given by

$$\bar{w}(\zeta)|_{(\zeta=0)} = 0, \quad (34)$$

$$\frac{d\bar{w}(\zeta)}{d\zeta}\Big|_{(\zeta=0)} = 0, \quad (35)$$

$$\left\{ \frac{d}{d\zeta} \left[g(\zeta) \frac{d^2\bar{w}(\zeta)}{d\zeta^2} \right] - s^2 h(\zeta) \frac{d\bar{w}(\zeta)}{d\zeta} + \frac{(s^2 + \lambda^2)}{r^2} g(\zeta) \frac{d\bar{w}(\zeta)}{d\zeta} \right\} \Big|_{(x=R)} = 0, \quad (36)$$

$$g(\zeta) \frac{d^2\bar{w}(\zeta)}{d\zeta^2} \Big|_{(x=R)} = 0. \quad (37)$$

From the weak formulation of Eq. (38), we can obtain the stiffness matrix as

$$[K] = \int_0^1 g(\zeta) \frac{d^2[N]^T}{d\zeta^2} \frac{d^2[N]}{d\zeta^2} d\zeta + \int_0^1 s^2 h(\zeta) \frac{d[N]^T}{d\zeta} \frac{d[N]}{d\zeta} d\zeta - \int_0^1 \frac{s^2}{r^2} g(\zeta) \frac{d[N]^T}{d\zeta} \frac{d[N]}{d\zeta} d\zeta \quad (38)$$

and the mass matrix as

$$[M] = \int_0^1 f(\zeta) [N]^T [N] d\zeta + \int_0^1 \frac{1}{r^2} g(\zeta) \frac{d[N]^T}{d\zeta} \frac{d[N]}{d\zeta} d\zeta. \quad (39)$$

7. Results

The results are obtained using 7 nodes within the sub-domain of trial function. First five natural frequencies along with the mode shapes are obtained. The results of the Euler-Bernoulli beam are also included for comparison. The results are in non-dimensional form; obtained for different rotating speeds of beam. The parameters which are used in non-dimensional form have been shown within the tables. The results are accurate when compared to the literature [25]. In tables, m is the number of nodes within the sub-domain of the trial function.

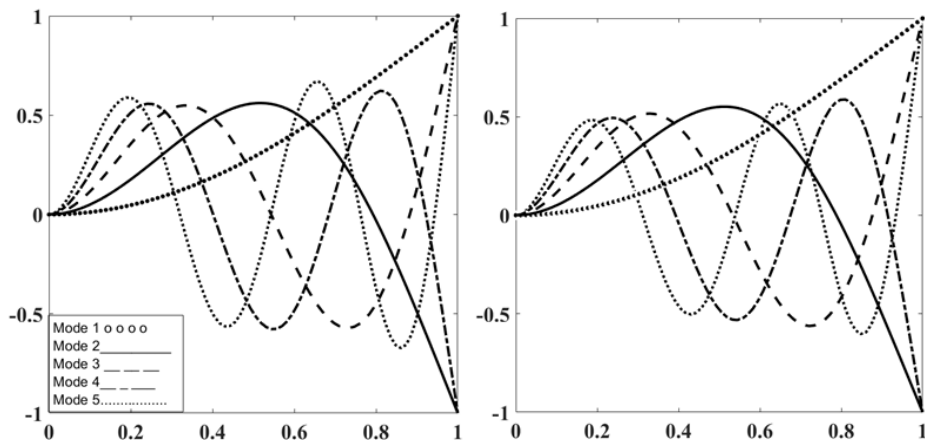
In Table 1 and Table 2 results are obtained using Chebyshev and Legendre polynomials, respectively. These results are for non-rotating beams. In Table 3

Table 1. Non-dimensional natural frequencies of a non-rotating Rayleigh beam

$r = 10, s = 0,$ $\bar{n} = 1, c = 1/2$			$r = 100, s = 0,$ $\bar{n} = 1, c = 1/2$		
	[25]	Chebyshev polynomials $m = 7$	[25]	Chebyshev polynomials $m = 7$	FEM ($n = 40$) (E-B)
λ_1	3.7727	3.7727	3.8233	3.8233	3.8238
λ_2	17.097	17.0975	18.304	18.3038	18.3173
λ_3	40.412	40.4127	47.178	47.1785	47.2649
λ_4	N/A	69.4379	N/A	90.1345	90.4509
λ_5	N/A	101.4728	N/A	147.2155	148.0035

Table 2. Non-dimensional natural frequencies of a non-rotating Rayleigh beam

$r = 10, s = 0,$ $\bar{n} = 1, c = 1/2$			$r = 100, s = 0,$ $\bar{n} = 1, c = 1/2$		
	[25]	Legendre polynomials $m = 7$	[25]	Legendre polynomials $m = 7$	FEM ($n = 40$) (E-B)
λ_1	3.7727	3.7727	3.8233	3.8233	3.8238
λ_2	17.097	17.0975	18.304	18.3038	18.3173
λ_3	40.412	40.4127	47.178	47.1785	47.2649
λ_4	N/A	69.4379	N/A	90.1345	90.4509
λ_5	N/A	101.4728	N/A	147.2155	148.0035

Fig. 4. Mode shapes of a non-rotating beam for $\bar{n} = 1, r = 10$ and $\bar{n} = 1, r = 100$, respectively

and Table 4 results are obtained using Chebyshev and Legendre polynomials, respectively. These results are for rotating beams. Respective mode shapes are shown in Fig. 4 and Fig. 5.

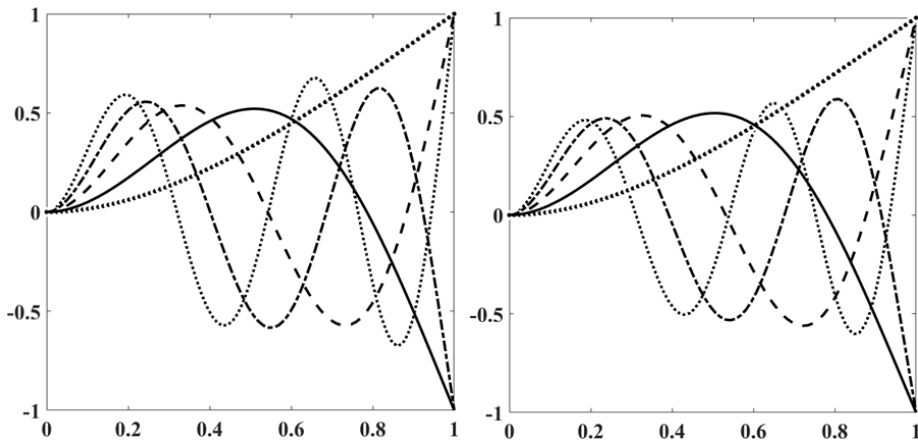
In Table 5 and Table 6 results are obtained using Chebyshev and Legendre polynomials, respectively. These results are for non-rotating beams. In Table 7

Table 3. Non-dimensional natural frequencies of a rotating Rayleigh beam

	$r = 10, s = 5,$ $\bar{n} = 1, c = 1/2$		$r = 100, s = 5,$ $\bar{n} = 1, c = 1/2$		
	[25]	Chebyshev polynomials $m = 7$	[25]	Chebyshev polynomials $m = 7$	FEM ($n = 40$) (E-B)
λ_1	6.6118	6.6118	6.7421	6.7421	6.7434
λ_2	20.356	20.3563	21.888	21.8882	21.9053
λ_3	43.444	43.4435	50.839	50.8392	50.9339
λ_4	N/A	72.2398	N/A	93.8774	94.2067
λ_5	N/A	104.0122	N/A	150.9873	151.8160

Table 4. Non-dimensional natural frequencies of a rotating Rayleigh beam

	$r = 10, s = 5,$ $\bar{n} = 1, c = 1/2$		$r = 100, s = 5,$ $\bar{n} = 1, c = 1/2$		
	[25]	Legendre polynomials $m = 7$	[25]	Legendre polynomials $m = 7$	FEM ($n = 40$) (E-B)
λ_1	6.6118	6.6118	6.7421	6.7421	6.7434
λ_2	20.356	20.3563	21.888	21.8882	21.9053
λ_3	43.444	43.4435	50.839	50.8392	50.9339
λ_4	N/A	72.2398	N/A	93.8774	94.2067
λ_5	N/A	104.0122	N/A	150.9873	151.8160

Fig. 5. Mode shapes of a rotating beam for $\bar{n} = 1, r = 10$ and $\bar{n} = 1, r = 100$, respectively

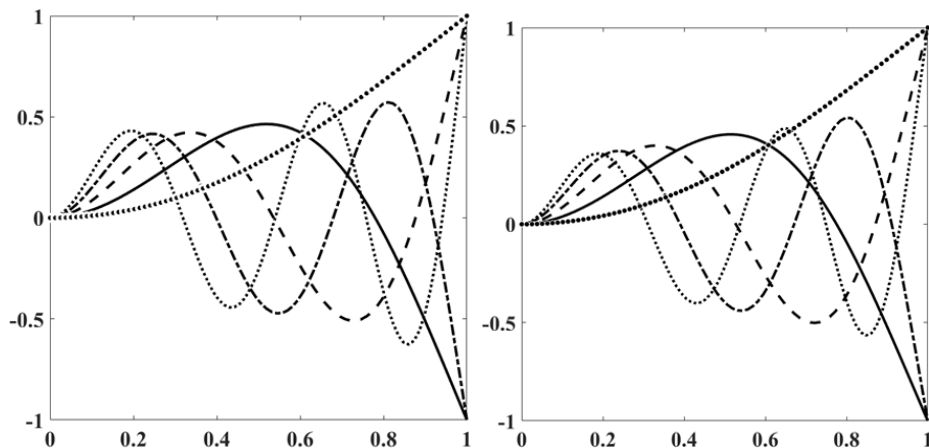
and Table 8 results are obtained using Chebyshev and Legendre polynomials, respectively. These results are for rotating beams. Respective mode shapes are shown in Fig. 6 and Fig. 7. In Fig. 8, the results are compared with non-rotating and rotating Euler-Bernoulli beams.

Table 5. Non-dimensional natural frequencies of a non-rotating Rayleigh beam

	$r = 10, s = 0,$ $\bar{n} = 2, c = 1/2$		$r = 100, s = 0,$ $\bar{n} = 2, c = 1/2$		
	[25]	Chebyshev polynomials $m = 7$	[25]	Chebyshev polynomials $m = 7$	FEM ($n = 40$) (E-B)
λ_1	4.5517	4.5517	4.6244	4.6244	4.6251
λ_2	18.211	18.2107	19.533	19.5328	19.5476
λ_3	41.457	41.4575	48.489	48.4891	48.5790
λ_4	N/A	70.3718	N/A	91.4898	91.8132
λ_5	N/A	102.2646	N/A	148.5339	149.3917

Table 6. Non-dimensional natural frequencies of a non-rotating Rayleigh beam

	$r = 10, s = 0,$ $\bar{n} = 2, c = 1/2$		$r = 100, s = 0,$ $\bar{n} = 2, c = 1/2$		
	[25]	Legendre polynomials $m = 7$	[25]	Legendre polynomials $m = 7$	FEM ($n = 40$) (E-B)
λ_1	4.5517	4.5517	4.6244	4.6244	4.6251
λ_2	18.211	18.2107	19.533	19.5328	19.5476
λ_3	41.457	41.4575	48.489	48.4891	48.5790
λ_4	N/A	70.3718	N/A	91.4898	91.8132
λ_5	N/A	102.2646	N/A	148.5339	149.3917

Fig. 6. Mode shapes of a non-rotating beam for $\bar{n} = 2, r = 10$ and $\bar{n} = 2, r = 100$, respectively

The maximum value of m is found to be seven in the case of both the polynomials (Chebyshev and Legendre). Above seven nodes, the matrix cannot be inverted and below seven the results will not be accurate. Above seven nodes, the matrix will be almost singular and ill-conditioned. The similar problem occurs in p-type of the finite element method where higher-order polynomials are used and numbers

Table 7. Non-dimensional natural frequencies of a rotating Rayleigh beam

	$r = 10, s = 5,$ $\bar{n} = 2, c = 1/2$		$r = 100, s = 5,$ $\bar{n} = 2, c = 1/2$		
	[25]	Chebyshev polynomials $m = 7$	[25]	Chebyshev Polynomials $m = 7$	FEM ($n = 40$) (E-B)
λ_1	7.1268	7.1268	7.2885	7.2885	7.2901
λ_2	21.003	21.0033	22.618	22.6179	22.6360
λ_3	44.014	44.0143	51.595	51.5947	51.6919
λ_4	N/A	72.7008	N/A	94.6285	94.9630
λ_5	N/A	104.3616	N/A	151.6834	152.5683

Table 8. Non-dimensional natural frequencies of a rotating Rayleigh beam

	$r = 10, s = 5,$ $\bar{n} = 2, c = 1/2$		$r = 100, s = 5,$ $\bar{n} = 2, c = 1/2$		
	[25]	Legendre polynomials $m = 7$	[25]	Legendre polynomials $m = 7$	FEM ($n = 40$) (E-B)
λ_1	7.1268	7.1268	7.2885	7.2885	7.2901
λ_2	21.003	21.0033	22.618	22.6179	22.6360
λ_3	44.014	44.0143	51.595	51.5947	51.6919
λ_4	N/A	72.7008	N/A	94.6285	94.9630
λ_5	N/A	104.3616	N/A	151.6834	152.5683

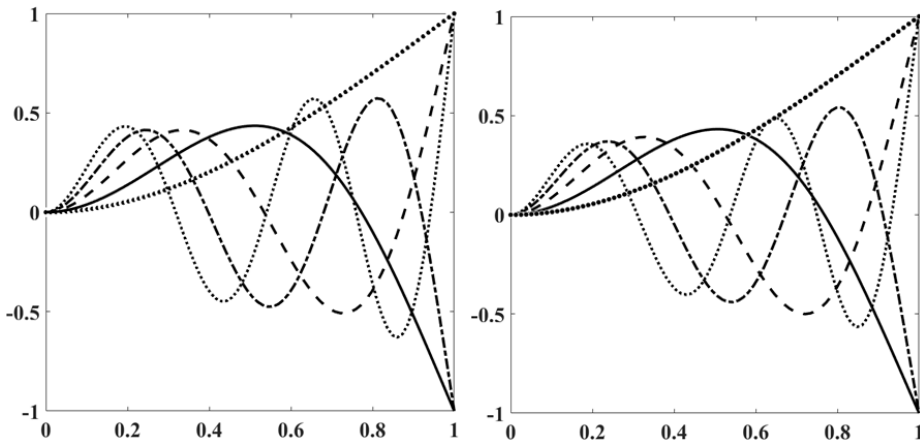


Fig. 7. Mode shapes of a rotating beam for $\bar{n} = 2, r = 10$ and $\bar{n} = 2, r = 100$, respectively

of nodes are considered within the element. Also, the Chebyshev and Legendre polynomials show the improvement over the conventional radial basis functions approximation where increased number of nodes can be included in the sub-domain of trial function.

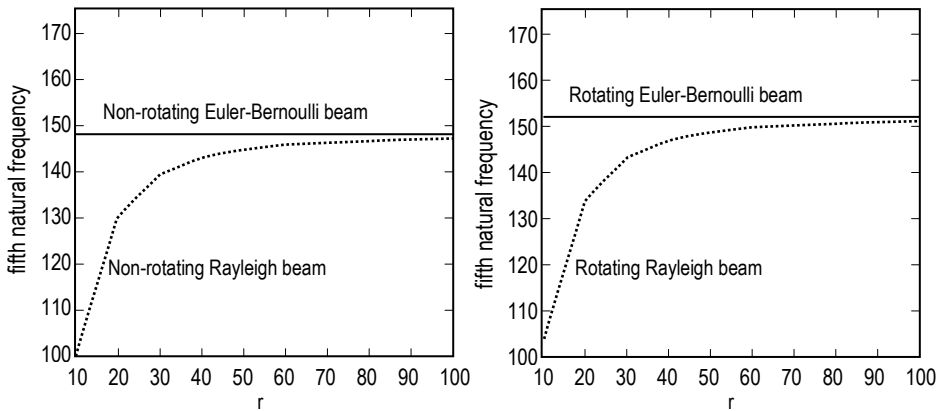


Fig. 8. Variation in the fifth natural frequency with change in the slenderness ratio for a non-rotating and a rotating beam, respectively

8. Conclusions

In this paper, the rotating Rayleigh beam problem has been solved with meshless local Petrov-Galerkin method where orthogonal polynomials are used: Chebyshev and Legendre polynomials. The number of nodes within the sub-domain can be increased when compared to the radial basis function. The formulation, which is completely explained, provides better results than the existing solutions with the meshless Petrov-Galerkin method. The first-five natural frequencies are calculated along with the respective mode shapes. The results are obtained for the 7 nodes within the sub-domain. The non-dimensional form has been explained in detail to compare the results. Also, results are compared with non-rotating and rotating Euler-Bernoulli beams.

References

- [1] R. Ganguli. *Finite Element Analysis of Rotating Beams*. Springer, Singapore, 2017.
- [2] R. Ganguli and V. Panchore. *The Rotating Beam Problem in Helicopter Dynamics*. Springer, Singapore, 2018.
- [3] S.N. Atluri. *The Meshless Method (MLPG) for Domain and BIE Discretizations*. Tech Science Press, Forsyth, 2004.
- [4] G.R. Liu. *Meshfree Methods*. CRC Press, New York, 2003.
- [5] I.S. Raju, D.R. Phillips, and T. Krishnamurthy. A radial basis function approach in the meshless local Petrov-Galerkin method for Euler-Bernoulli beam problems. *Computational Mechanics*, 34:464–474, 2004. doi: [10.1007/s00466-004-0591-z](https://doi.org/10.1007/s00466-004-0591-z).
- [6] D. Hu, Y. Wang, Y. Li, Y. Gu and X. Han. A meshfree-based local Galerkin method with condensation of degree of Freedom. *Finite Elements in Analysis and Design*, 78:16–24, 2014. doi: [10.1016/j.finel.2013.09.004](https://doi.org/10.1016/j.finel.2013.09.004).

- [7] S. De Marchi and M.M. Cecchi. The polynomial approximation in finite element method. *Journal of Computational and Applied Mathematics*, 57(1-2):99–114, 1995. doi: [10.1016/0377-0427\(93\)E0237-G](https://doi.org/10.1016/0377-0427(93)E0237-G).
- [8] V. Panchore, R. Ganguli, and S.N. Omkar. Meshless local Petrov-Galerkin method for rotating Euler-Bernoulli beam. *Computer Modeling in Engineering and Sciences*, 104(5):353–373, 2015. doi: [10.3970/cmcs.2015.104.353](https://doi.org/10.3970/cmcs.2015.104.353).
- [9] V. Panchore, R. Ganguli, and S.N. Omkar. Meshless local Petrov-Galerkin method for rotating Timoshenko beam: a locking-free shape function formulation. *Computer Modeling in Engineering and Sciences*, 108(4):215–237, 2015. doi: [10.3970/cmcs.2015.108.215](https://doi.org/10.3970/cmcs.2015.108.215).
- [10] W. Johnson. *Helicopter Theory*. Dover Publications, New York, 1980.
- [11] A. Bokaian. Natural frequencies of beams under tensile axial loads. *Journal of Sound and Vibration*, 142(3):481–498, 1990. doi: [10.1016/0022-460X\(90\)90663-K](https://doi.org/10.1016/0022-460X(90)90663-K).
- [12] S.V. Hoa. Vibration of a rotating beam with tip mass. *Journal of Sound and Vibration*, 67(3):369–381, 1979. doi: [10.1016/0022-460X\(79\)90542-X](https://doi.org/10.1016/0022-460X(79)90542-X).
- [13] H.D. Hodges and M.J. Rutkowski. Free-vibration analysis of rotating beams by a variable-order finite element method. *AIAA Journal*, 19(11):1459–1466, 1981. doi: [10.2514/3.60082](https://doi.org/10.2514/3.60082).
- [14] J. Chung and H.H. Yoo. Dynamic analysis of a rotating cantilever beam by using the finite element method. *Journal of Sound and Vibration*, 249:147–164, 2002. doi: [10.1006/jsvi.2001.3856](https://doi.org/10.1006/jsvi.2001.3856).
- [15] R.L. Bisplinghoff, H. Ashley, and R.L. Halfman. *Aeroelasticity*. Dover Publications, New York, 1996.
- [16] V. Giurgiutiu and R.O. Stafford. Semi-analytical methods for frequencies and mode shapes of rotor blades. *Vertica*, 1:291–306, 1977.
- [17] J.B. Gunda and R. Ganguli. Stiff-string basis functions for vibration analysis of high speed rotating beams. *Journal of Applied Mechanics*, 75(2):0245021, 2008. doi: [10.1115/1.2775497](https://doi.org/10.1115/1.2775497).
- [18] V. Panchore and R. Ganguli. Quadratic B-spline finite element method for a rotating non-uniform Rayleigh beam. *Structural Engineering and Mechanics*, 61(6):765–773, 2017. doi: [10.12989/sem.2017.61.6.765](https://doi.org/10.12989/sem.2017.61.6.765).
- [19] V. Panchore and R. Ganguli. Quadratic B-spline finite element method for a rotating non-uniform Euler-Bernoulli beam. *International Journal for Computational Methods in Engineering Science and Mechanics*, 19(5):340–350, 2018. doi: [10.1080/15502287.2018.1520757](https://doi.org/10.1080/15502287.2018.1520757).
- [20] T. Rabczuk, J-H Song, X. Zhuang, and C. Anitescu. *Extended Finite Element and Meshfree Methods*. Elsevier, London, 2020.
- [21] J.R. Xiao and M.A. McCarthy. Meshless analysis of the obstacle problem for beams by the MLPG method and subdomain variational formulations. *European Journal of Mechanics - A/Solid*, 22(3):385–399, 2003. doi: [10.1016/S0997-7538\(03\)00050-0](https://doi.org/10.1016/S0997-7538(03)00050-0).
- [22] J.Y. Cho and S. N. Atluri. Analysis of shear flexible beams, using the meshless local Petrov-Galerkin method, based on a locking-free formulation. *Engineering Computations*, 18(1-2):215–240, 2001. doi: [10.1108/02644400110365888](https://doi.org/10.1108/02644400110365888).
- [23] J. Sladek, V. Sladek, S. Krahulec, and E. Pan. The MLPG analyses of large deflections of magneto-electroelastic plates. *Engineering Analysis with Boundary Elements*, 37(4):673–682, 2013. doi: [10.1016/j.enganabound.2013.02.001](https://doi.org/10.1016/j.enganabound.2013.02.001).
- [24] S.N. Atluri, J.Y. Cho, and H.-G. Kim. Analysis of thin beams, using the meshless local Petrov-Galerkin method, with generalized moving least squares interpolations. *Computational Mechanics*, 24:334–347, 1999. doi: [10.1007/s004660050456](https://doi.org/10.1007/s004660050456).
- [25] J.R. Banerjee and D.R. Jackson. Free vibration of a rotating tapered Rayleigh beam: A dynamic stiffness method of solution. *Computers and Structures*, 124:11–20, 2013. doi: [10.1016/j.compstruc.2012.11.010](https://doi.org/10.1016/j.compstruc.2012.11.010).